Influence of the *R*(61,2)- and *S*(61,2)-α-(*N*^{6}-Adenyl)styrene Oxide Adducts on the A·C Mismatched Base Pair in an Oligodeoxynucleotide Containing the Human *N-ras* Codon 61†

Sherry L. Painter,‡ Irene S. Zegar,§ Pamela J. Tamura, Susanna Bluhm, Constance M. Harris, Thomas M. Harris, and Michael P. Stone*

Department of Chemistry and Center in Molecular Toxicology, Vanderbilt University, Nashville, Tennessee 37235

Received January 6, 1999; Revised Manuscript Received April 22, 1999

ABSTRACT: Conformational studies of *R*- and *S*-α-(*N*^{6}-adenyl)styrene oxide adducts mismatched with deoxycytosine at position X^6 in d(CGGACXAGAAG)·d(CTTCTCGTCCG), incorporating codons 60, 61 (underlined), and 62 of the human *N-ras* protooncogene, are described. These were the R- and S(61,2)C adducts. The S(61,2)C adduct afforded a stable solution structure, while the R(61,2)C adduct resulted in a disordered structure. Distance restraints for the S(61,2)C adduct were calculated from NOE data using relaxation matrix analysis. These were incorporated as effective potentials into the total energy equation. The structures were refined using restrained molecular dynamics calculations which incorporated a simulated annealing protocol. The accuracy of the emergent structures was evaluated by complete relaxation matrix methods. The structures refined to an average rms difference of 1.07 Å, determined by pairwise analysis. The experimentally determined structure was compared to NOE intensity data using complete relaxation matrix back-calculations, yielding an R_1^x value of 11.2×10^{-2}. The phenyl ring of the styrene in the S(61,2)C adduct was in the major groove and remained oriented in the 3′-direction as observed for the corresponding S(61,2) adduct paired with thymine [Feng, B., Zhou, L., Pasarelli, M., Harris, C. M., Harris, T. M., and Stone, M. P. (1995) *Biochemistry 34*, 14021−14036]. A shift of the modified adenine toward the minor groove resulted in the styrenyl ring stacking with nucleotide C^5 on the 5′-side of the lesion, which shifted toward the major groove. Unlike the unmodified A·C mismatch, neither the S(61,2)C nor the R(61,2)C adduct formed protonated wobble A·C hydrogen bonds. This suggests that protonated wobble A·C pairing need not be prerequisite to low levels of α-SO-induced A → G mutations. The shift of the modified adenine toward the minor groove in the S(61,2)C structure may play a more important role in the genesis of A → G mutations. The disordered structure of the R(61,2)C adduct provides a potential explanation as to why that adduct does not induce A → G mutations.

Styrene, a mutagen in prokaryotes (*1, 2*) and eukaryotes (*3*), is of concern as a potential human mutagen (*4*−*7*), as a consequence of chronic occupational exposure to styrene, particularly in the manufacture of reinforced plastics by lamination. Styrene genotoxicity results from cytochrome P$_{450}$-mediated metabolism to the ultimate carcinogenic species, styrene oxide (SO)[1] (*8*−*15*). The oxide reacts in vitro to form adducts at a number of nucleophilic sites in DNA, including the *R*- and *S*-enantiomers at the exocyclic amino groups of guanine (*16*) and adenine (*17*). The adenyl N^6 adducts arise in vitro both from direct reaction at the exocyclic carbon and as a consequence of Dimroth rearrangement following reaction at N1 (*18*) (Scheme 1). The reaction of styrene oxides with the exocyclic amino groups of guanosine (*19*) and adenine (*18*) exhibited considerable S$_N$1 character, but favored inversion of stereochemistry.

Adducts of SO at guanine O^6 and guanine N^2 have been identified in human cells (*20*−*23*). Increased levels of the guanine O^6 adduct, a biomarker for styrene, were observed in styrene-exposed lamination workers (*24*). SO was a weak

† This research was supported by NIH Grant ES-05509 (M.P.S.). Funding for the NMR spectrometer was supplied by a grant from the NIH shared instrumentation program (RR-05805) and the Vanderbilt Center in Molecular Toxicology (ES-00267). This study made use of the National Magnetic Resonance Facility at Madison. NMRFAM equipment was purchased with funds from the University of Wisconsin, NSF Grants DMB-8415048 and BIR-9214394, NIH Grants RR-02301, RR-02781, and RR08438, and the USDA.

* To whom correspondence should be addressed. Phone: (615) 322-2589. Fax: (615) 343-1234 E-mail: stone@toxicology.mc.vanderbilt.edu.

‡ Current address: Division of Science, Volunteer State Community College, Gallatin, TN 37066.

§ Current Address: Department of Chemistry, Pittsburg, State University, Pittsburg, KS 66762.

[1] Abbreviations: DSS, 2,2-dimethyl-2-silapentane-5-sulfonate; EDTA, ethylenediaminetetraacetic acid; HPLC, high-pressure liquid chromatography; MD, molecular dynamics; rMD, restrained molecular dynamics; NMR, nuclear magnetic resonance; NOE, nuclear Overhauser enhancement; NOESY, two-dimensional NOE spectroscopy; PAH, polycyclic aromatic hydrocarbon; ppm, parts per million; SO, styrene oxide; TPPI, time proportional phase increment; TOCSY, total homonuclear correlated spectroscopy; 1D, one-dimensional; 2D, two-dimensional; A, C, G, T, mononucleotide units; $^{R-SO}$A, *R*-α-styrene oxide modified nucleotide; $^{S-SO}$A, *S*-α-styrene oxide modified nucleotide. A right superscript refers to the numerical position in the oligodeoxynucleotide sequence starting from the 5′-terminus of chain A and proceeding to the 3′-terminus of chain A and then from the 5′-terminus of chain B to the 3′-terminus of chain B.

10.1021/bi9900323 CCC: $18.00
Published on Web 06/17/1999

Scheme 1: R(61,2)C and S(61,2)C Mismatched Oligodeoxynucleotides[a]

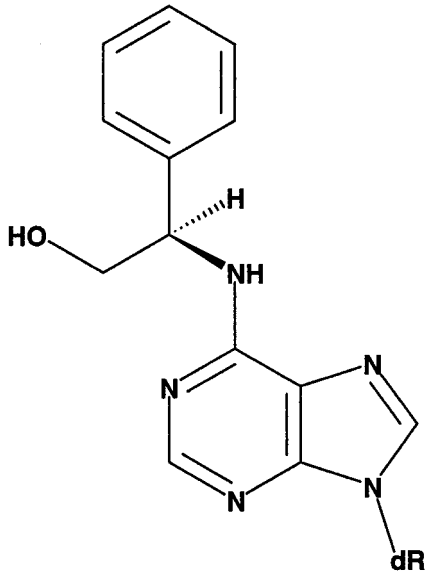

R-α-(N⁶-adenyl)-styrene oxide adduct

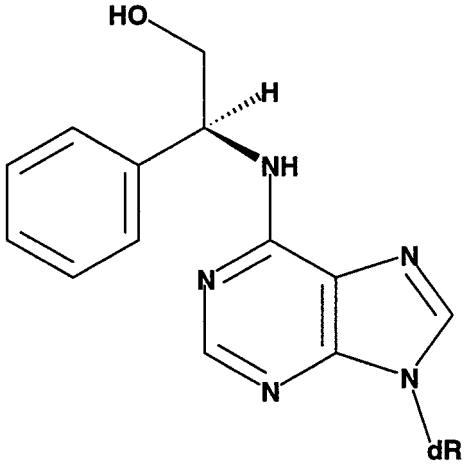

S-α-(N⁶-adenyl)-styrene oxide adduct

[a] R = *R*-α-(*N*⁶-adenyl)styrene oxide and S = *S*-α-(*N*⁶-adenyl)styrene oxide adduct. The mismatched SO-adducted oligodeoxynucleotides were compared to the corresponding A·C mismatch at position (61,2).

mutagen at the hypoxanthine−guanine phosphoribosyl transferase (*hprt*) gene in peripheral blood lymphocytes. Molecular analysis of the *hprt* mutations suggested that they occurred at both guanine and adenine sites, and were predominantly base pair substitutions (*25*). However, the levels of guanine O^6 adducts and the frequencies of *hprt* mutations did not show a strong correlation (*24*). This suggested that these SO adducts were weakly mutagenic or perhaps not the source of the mutations. Alternatively, it could suggest that a simple quantitative relationship did not exist between styrene-induced DNA damage and mutagenesis (*23*). SO also induces sister chromosome exchange and aberrations in human lymphocytes in vitro (*26, 27*).

We have focused attention on the *R*- and *S*-α-SO adducts located at the exocyclic amino groups of adenines in the codon 61 sequence of the human *N-ras* protooncogene. Site-specific mutagenesis studies performed by R. S. Lloyd and co-workers on the *ras61* sequence with the S-SO moiety adducted at the S(61,2) position revealed that the adenyl N^6 lesion was weakly mutagenic, giving rise to low levels of A → G transitions (*28*). Interestingly, this was the dominant SO-induced *hprt* mutation in human lymphocytes (*25*). Thus, while the guanine O^6 adducts provided a biomarker, the adenine N^6 lesions might be more mutagenic (*25*). While the adenyl N^6 α-SO adducts were weakly mutagenic, the bulkier intercalating adenyl N^6 adducts of benzo[*a*]pyrene (*29*) and benz[*a*]anthracene (*30*) also yielded A → G mutations, but at greater levels. To develop a better understanding of the relationship between adduct structure and activity at adenine N^6, it was of interest to examine whether a structural basis could be discerned for the induction of A → G mutations by SO. Explanations included the possibilities that SO adduction (1) facilitated formation of wobble pairing between protonated adenine and cytosine (*31*−*42*), or (2) perturbed the geometry of the adducted adenine so that the replication complex misinserted cytosine.

The *ras61* oligodeoxynucleotide provides a model for examining the structural consequences of site-specific DNA adduction by SO. The structures of the *ras61* oligodeoxynucleotide d(CGGACAAGAAG)·d(CTTCTTGTCCG) (*43*) and the *R*- and *S*-(61,2)-α-styrene oxide lesions in the *ras61* oligodeoxynucleotide (*44*−*46*) revealed the influence of stereochemistry in determining the major groove orientation of α-SO adducts at adenine N^6, with the *R*-diastereomer being oriented in the 5′-direction while the *S*-diastereomer was oriented in the 3′-direction from the lesion site. Tumor cell genomes often, but not always, contain mutations in *ras*. Mutations in *ras* are commonly observed in pancreatic cancer (*47*). Potential SO-induced mutations in *ras* are expected to contribute to cellular transformation. However, the contemporary view of carcinogenesis as a multistep process (*48, 49*) suggests that identifying the precise biological consequences of specific SO-induced mutations will be difficult. The biology may differ from one cell to the next, depending upon the overall genetic background of the specific somatic cells in which the mutations occur. Mutations potentially induced by SO will not necessarily be rate-limiting in carcinogenesis. It seems likely that both the nature and sequential order of genetic changes modulate tumor morphology and the likelihood of tumor progression (*50*).

This report describes conformational studies of *R*- and *S*-α-(*N*⁶-adenyl)styrene oxide adducts mismatched with deoxycytosine at position X^6 in d(CGGACXAGAAG)·d(CTTCTCGTCCG), incorporating codons 60, 61 (underlined), and 62 of the human *N-ras* protooncogene. These are designated as the R- and S(61,2)C adducts, indicating their stereochemistry and location at the second nucleotide in codon 61. The unmodified A·C mismatch at position (61,2) served as a reference (Scheme 2). Surprisingly, and unlike the *ras61* unmodified (61,2) A·C mismatch, neither the R- nor the S(61,2)C SO adducts formed protonated A·C pairs. Furthermore, ^{1}H NMR spectroscopy and UV melting data revealed that unlike the R(61,2) adduct which existed as a single conformation in which the styrenyl moiety was oriented in the 5′-direction in the major groove from the lesion site (*44, 46*), the R(61,2)C adduct was disordered. In contrast, the S(61,2)C adduct now existed as a single species in solution, and yielded a refined solution structure, whereas the S(61,2) adduct had equilibrated between multiple conformations (*45, 46*). The NOESY data revealed that the

Scheme 2: Structures of the *R*- and *S*-α-(*N*^{6}-Adenyl)styrene Oxide Adducts

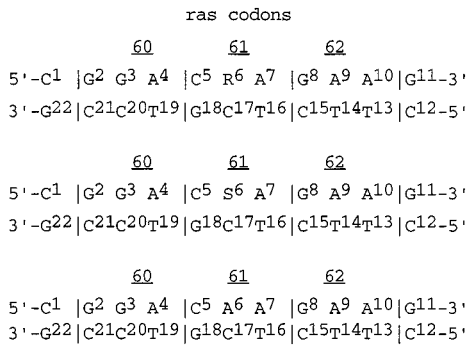

phenyl ring of the styrene moiety was located in the major groove of the DNA and oriented in the 3′-direction. A shift of the modified adenine toward the minor groove resulted in the styrenyl ring stacking with nucleotide C^5 on the 5′-side of the lesion, which had shifted toward the major groove. This adduct-induced change in base-pairing geometry provides a possible explanation for the low levels of A → G mutations observed for the S(61,2) adduct, which were not observed for the R(61,2) adduct (*28*).

MATERIALS AND METHODS

Oligonucleotide Preparation. The unmodified oligodeoxynucleotide 5′-d(CGGACAAGAAG)-3′ and its mismatch complement 5′-d(CTTCTCGTCCG)-3′ were purchased from the Midland Certified Reagent Co. (Midland, TX). The SO-adducted oligodeoxynucleotides were prepared and purified as reported (*51*). Enzyme digest and circular dichroism (CD) analyses were performed to verify the stereochemistry of the adducted oligodeoxynucleotides. The concentrations of the single-stranded oligodeoxynucleotides were determined from the extinction coefficients (*52*), 9.71×10^{-4} and 8.73×10^4 M^{-1} cm^{-1}, respectively. Equimolar amounts were mixed and annealed in 10 mM NaH_2PO_4, 0.1 M NaCl, and 50 μM Na_2-EDTA at pH 6.9. The annealed duplex was eluted from a hydroxylapatite column using sodium phosphate. The samples were desalted using gel filtration (BioGel G-25, BioRad, Inc., Hercules, CA).

UV−Vis Spectroscopy. UV melting studies were performed on a Cary 4E (Varian Associates, Palo Alto, CA) spectrophotometer interfaced with a Cary variable temperature controller. The data were collected over a range of 5−90 °C at a temperature rise of 1 °C/min. The samples were dissolved in 1.0 M NaCl, 0.01 M NaH_2PO_4, and 0.05 mM Na_2EDTA buffer at pH 5.0, 7.0, and 8.5. Optical measurements were recorded at 260 nm.

NMR. Samples were buffered in 0.1 M NaCl, 0.01 M NaH_2PO_4, and 0.05 mM Na_2EDTA, at the indicated pH values. For observation of nonexchangeable ^{1}H resonances, the SO-adducted samples were repeatedly lyophilized and then dissolved in 0.25 mL of 99.996% D_2O to yield a 1.5 mM solution using a Shigemi (Shigemi, Inc., Allison Park, PA) microtube. For observation of exchangeable protons, the samples were dissolved in 0.25 mL of a 9:1 H_2O/D_2O buffer of the same composition. For pH titration work using NMR, the oligodeoxynucleotides were dissolved in 0.01 M NaH_2PO_4 buffer containing 0.1 M NaCl and 0.05 mM Na_2EDTA at pH 5.0. The chemical shift of the adenine H8 resonance in the A·C mismatched pair was recorded over a pH range of 4.5−8.5. One-dimensional spectra were recorded except in several instances when the H8 resonance was overlapped with other signals; in these instances it was identified from NOESY data. The titration was carried out in the NMR tube, and the pH of the sample was monitored directly with a 180 × 3 mm micro electrode (Ingold Electrodes, Inc., Wilmington, MA). The titrants were 0.4% NaOD and 0.5% DCl in D_2O. For assignment purposes, spectra of the unmodified (61,2)C mismatched duplex, the S(61,2)C adduct, and the R(61,2)C adduct were recorded at a ^{1}H frequency of 750.13 MHz. Phase-sensitive NOESY spectra in D_2O, used for the assignments of the nonexchangeable protons and subsequently for distance measurement, were recorded using the standard pulse sequence and the TPPI method for quadrature detection with mixing times of 150, 250, and 350 ms. The residual water resonance was saturated during the relaxation delay and the mixing period. 1D experiments in 90% H_2O were carried out using a jump return 1−1 echo pulse sequence for water suppression (*53*). Phase-sensitive NOESY experiments in 90% H_2O were carried out using a jump return 1−1 sequence as the read pulse for water suppression (*54, 55*). Convolution difference was used during processing to minimize the residual water signal (*56*). The data were processed using FELIX950 (Molecular Simulations, Inc., San Diego, CA), running on Indigo^2 workstations (Silicon Graphics, Inc., Mountain View, CA). Chemical shifts were referenced internally to the residual water resonance. The data were processed with a shifted skewed sinebell squared apodization function using a phase angle of 90° and a skew factor of 0.7.

Distance Restraints. Footprints were selected manually with FELIX950 to fit NOE cross-peaks at the contour level chosen which showed the weak NOEs but not the random noise. NOE cross-peaks were integrated for the three sets of spectra using the same contour levels. For overlapped cross-peaks, footprints were estimated, and larger upper and lower error bounds were assigned to the resulting distances. Canonical A- and B-DNA oligodeoxynucleotides were generated using INSIGHTII (Molecular Simulations, Inc., San Diego, CA) and served as reference structures for establishing an initial intensity matrix. The styrene moiety was incorporated into these initial structures by bonding the benzylic carbon of styrene oxide, with appropriate stereochemistry, to the N^6 of adenine. These structures were energy minimized, using X-PLOR (*57*), for 100 iterations by the conjugate gradient method to give the starting structures IniA and IniB. For each of the three mixing times, the experimental NOE derived distances were combined with the initial intensity matrix to generate a hybrid intensity matrix using MARDIGRAS (*58*). Calculations were run using correlation times, τ_c, of 2, 3, 4, and 5 ns, at each NOE mixing time. The 12 resulting distance sets were pooled; average values of all minimum and maximum distances were used in setting error bounds to give the experimental NOE restraints used in subsequent molecular dynamics calculations (*59*). Overlap of the aromatic resonances prevented complete assignments of the styrene protons for the S(61,2)C adduct and hindered accurate volume integration. Inspection of molecular models predicted the magnitudes of expected NOEs between styrene aromatic protons and DNA. Overlapped cross-peaks between styrene and DNA protons in the modified strand were not

included in the NOE intensities used by MARDIGRAS. They were assumed to include both first- and second-order contributions from $H_{o'}$, $H_{m'}$, and H_p. Distances between the styrene and DNA protons obtained from model structures were assigned as strong, medium, and weak restraints in MD calculations, with ranges 1.8−3.0 Å, 3.0−4.0 Å, and >4.0 Å, respectively.

Molecular Dynamics. Calculations were carried out using X-PLOR. The total energy was the sum of the empirical energy of the molecule and the effective energy. The empirical energy was derived from the CHARMM force field (*60*) developed for nucleic acids, and treated all hydrogens explicitly. The empirical energy consisted of the energy terms for bonds, bond angles, dihedral angles, chirality or planarity, hydrogen bonding, and nonbonded interactions. The nonbonded interactions included van der Waals and electrostatic terms, which used the pure Lennard−Jones and coulomb functions, respectively. The electrostatic term was based on a reduced charge set of partial charges (−0.32/residue) and a dielectric constant of 4.0. The cutoff radius for nonbonded interactions was 11 Å, and the nonbonded list was updated if any atom moved more than 0.5 Å. The SHAKE algorithm (*61*) was used to fix all bond lengths involving hydrogens. The effective energy was comprised of two terms describing the distance and dihedral restraints (E_{dist} and E_{dihe}), which utilized square well potentials. Empirical base-pairing distance and planarity restraints were used as follows: for G·C base pairs, r(cytosine N^4−guanosine O^6) = 2.91 ± 0.05 Å, r(cytosine N3−guanosine N1) = 2.95 ± 0.05 Å, r(cytosine O^2−guanosine N^2) = 2.86 ± 0.05 Å, r(cytosine N3−guanosine N^2) = 3.65 ± 0.05 Å, r(cytosine O^2−guanosine O^6) = 5.42 ± 0.05 Å; for A·T base-pairs, r(adenosine N^6−thymidine O^4) = 2.95 ± 0.05 Å, r(adenosine N1−thymidine N3) = 2.82 ± 0.05 Å, r(adenosine N1−thymidine O^4) = 3.63 ± 0.05 Å, r(adenosine N^6−thymidine O^2) = 5.40 ± 0.05 Å. The value of the torsion angle for the Watson−Crick base pair was (purine C2−purine N1−pyrimidine N3−pyrimidine C2) = 0 ± 10°. Empirical base step distances were r(H8−H8) = 5.00 ± 0.20 Å, r(H6−H6) = 5.00 ± 0.20 Å, and r(H8−H6) = 4.80 ± 0.20 Å.

A set of 5 rMD calculations were carried out using both IniA and IniB as starting structures. The system was coupled to a temperature bath with a target temperature of 900 K which was reached in 3 ps and maintained for 17 ps. The force constants of the experimental and empirical restraints were modulated over the course of the simulated annealing protocol by applying scale factors. Specifically, the four classes of NOE restraints were scaled up for 3.5 ps during the heating period to 150, 120, 90, and 60 kcal/(mol·Å^2) (best to worst class, respectively). These weights were maintained for the duration of the heating period and into the first 2 ps of the equilibrium dynamics period and were subsequently scaled back down to their original values. The dihedral and base pair restraints were also modulated during the simulated annealing. When the NOE force constants were scaled up, the dihedral and base pair force constants were scaled up to 100 kcal/(mol·Å^2) and then scaled back down to 20 kcal/(mol·Å^2) when the NOE restraints were scaled down. The system was then allowed to cool to 300 K over a 3 ps time period and maintained at 300 K for 25 ps. Coordinate sets were archived every 0.1 ps. The emergent structures from the last 5 ps were averaged and energy minimized for 300 iterations by the conjugate gradient method to yield the final structures. The integration time step was 1 fs. Structure coordinates were archived every 0.1 ps. Back-calculation of theoretical NOE intensities was carried out using CORMA (*62*). The refined structures were analyzed using DIALS & WINDOWS 1.0 (*63*).

Table 1: T_m Values for the *ras61* Oligodeoxynucleotide, Various (61,2)-α-SO Modifications, and the R- and S-α-(61,2)C Mismatched Oligodeoxynucleotides

oligodeoxynucleotide duplex	T_m (±1 °C)
ras61	53
R(61,2)	44
S(61,2)	37
(61,2)C	38
R(61,2)C	33
S(61,2)C	32

RESULTS

Thermodynamic Stability. The T_m values of the (61,2)C mismatch and the adducted R(61,2)C, and S(61,2)C mismatches were determined by UV analysis (Table 1), and compared with the corresponding duplexes not containing the mismatched cytosine. Both the R- and S(61,2)C mismatches exhibited similar T_m values of 32 and 33 °C, respectively. The cytosine mismatch reduced the stability of the R- and S(61,2)C mismatches as compared to the corresponding R- or S(61,2) adducted duplexes, which exhibited T_m values of 44 and 37 °C, respectively. The similar T_m values for both the R- and S(61,2)C mismatches contrasted with the corresponding nonmismatched α-SO adducts, for which the R(61,2) adduct was more stable, with a 7 °C greater T_m. The increased stability of the R(61,2) adduct as compared to the S(61,2) adduct was correlated with the observation that the R(61,2) adduct formed a single structure in which the styrenyl moiety was oriented in the 5′-direction in the major groove, while the S(61,2) adduct was disordered, with the primary conformation having the styrenyl moiety oriented in the 3′-direction in the major groove (*46*). Thus, formation of the cytosine mismatch destabilized the S(61,2) adduct to a lesser extent than the R(61,2) adduct.

pH Dependence. The formation of the A·C mismatch was anticipated to be dependent upon pH, due to the potential for formation of protonated wobble pairing between the mismatched bases (*31*−*42*). Accordingly, ^{1}H NMR spectra of the (61,2)C mismatch and of the R- and S(61,2)C mismatches were recorded as a function of pH. The ^{1}H spectrum of both the R(61,2)C and S(61,2)C mismatched adducts showed no change with pH in the range of 4.5−8.5. The NMR results were corroborated by UV studies, which showed a decrease in T_m at lower pH values. Thus, the conformations of the R(61,2)C and S(61,2)C adducts were examined at pH 7.0. The unadducted (61,2)C duplex did exhibit the anticipated pH dependence. Lowering the pH to 5.2 resulted in a sharpening of the proton resonances associated with the adenine and cytosine of the mismatch and the 5′ neighboring C·G base pair. The unmodified (61,2)C mismatched duplex was therefore examined at pH 5.2. The NMR data associated with the (61,2)C duplex were fully consistent with formation of protonated wobble pairing as has been observed for a number of other A·C mismatches

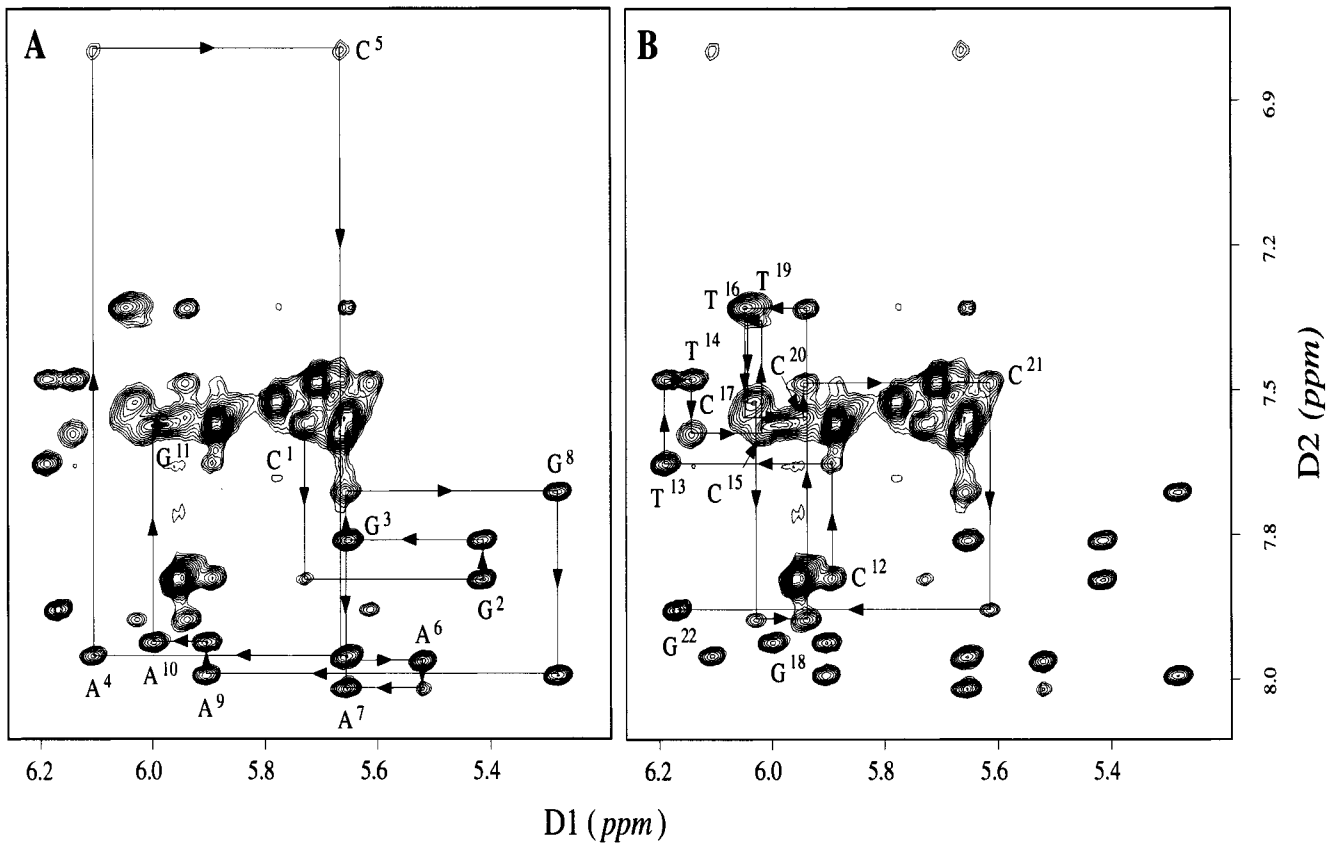

FIGURE 1: Expanded plot of a phase-sensitive NOESY spectrum in D_2O buffer for the S(61,2)C adduct (pH 7.0) at a mixing time of 350 ms showing the sequential NOE connectivities from the aromatic to anomeric protons. (A) Sequential NOE connectivities for nucleotides $C^1 \rightarrow G^{11}$. (B) Sequential NOE connectivities for nucleotides $C^{12} \rightarrow G^{22}$. The base positions are indicated at the intranucleotide cross-peak of the aromatic proton to its own anomeric proton.

in oligodeoxynucleotide duplexes; consequently, in the following sections the NMR results for this duplex will be omitted. The interested reader is referred to the Supporting Information for an accounting of this work.

Nonexchangeable Proton Assignments. (a) The R(61,2)C Mismatch at pH 7. This sample showed moderate levels of resonance overlap in the anomeric and aromatic regions of the ^{1}H spectrum used for analysis of NOE sequential connectivities (*64*, *65*), similar to the *ras61* oligomer (*43*). However, interruptions were observed in the sequential assignment scheme from $A^4 \rightarrow {}^{R-SO}A^6$ and from $C^{15} \rightarrow G^{18}$. The A^4 H1′ $\rightarrow$ C^5 H6, C^5 H6 $\rightarrow$ C^5 H1′, and C^5 H1′ $\rightarrow$ ${}^{R-SO}A^6$ H8 connectivities were not observed. The ${}^{R-SO}A^6$ H8 $\rightarrow$ ${}^{R-SO}A^6$ H1′ cross-peak was weak, and the ${}^{R-SO}A^6$ H1′ $\rightarrow$ A^7 H8 cross-peak was barely detectable. The A^7 H8 $\rightarrow$ A^7 H1′ and A^7 H1′ $\rightarrow$ G^8 H8 cross-peaks were also weak. The remaining cross-peaks in the adducted strand were of normal intensity. In the complimentary strand, the C^{15} H1′ $\rightarrow$ T^{16} H6, T^{16} H6 $\rightarrow$ C^{17} H1′, and C^{17} H1′ $\rightarrow$ G^{18} H8 connectivities were not observed. The scalar connectivities between C^5 H5 and C^5 H6, and C^{17} H5 and C^{17} H6 were also not observable. However, the resonance for C^5 H5 was identified, shifted upfield by ~1.7 ppm with respect to the (61,2)C adduct. Table S1 in the Supporting Information lists the chemical shifts of the nonexchangeable protons of the R(61,2)C adduct.

(b) The S(61,2)C Mismatch. This sample also showed moderate levels of resonance overlap in the anomeric and aromatic regions of the ^{1}H spectrum used for analysis of NOE sequential connectivities, again similar to the *ras61* oligomer (*43*). A complete set of sequential connectivities was obtained (Figure 1). The A^4 H1′ $\rightarrow$ C^5 H6 and C^5 H6 $\rightarrow$ C^5 H1′ cross-peaks were broadened. All of the other resonances were sharp. The chemical shift of the C^5 H5 and H6 protons was noteworthy. C^5 H5 shifted upfield 0.4 ppm and C^5 H6 shifted upfield 1.1 ppm from what was observed in the spectrum of the unmodified (61,2)C sample. Table S2 in the Supporting Information lists the chemical shifts of the nonexchangeable protons of the S(61,2)C adduct.

Exchangeable Proton Assignments. (a) The R(61,2)C mismatch. The cross-peaks in the imino region showed connectivites between $G^2 \rightarrow G^3 \rightarrow T^{19} \rightarrow G^{18}$ and $G^8 \rightarrow T^{14} \rightarrow T^{13}$. No imino resonance was observed for the mismatched ${}^{R-SO}A^6 \cdot C^{17}$ base pair. The T^{16} imino proton on the 3′-side of the mismatch was identified from an exchange peak with the water but did not show an NOE to G^8 N1H, suggesting that it was rapidly exchanging. The imino protons of the terminal $C^1 \cdot G^{22}$ and $G^{11} \cdot C^{12}$ base pairs, which exhibited fast exchange with the solvent, were not detected. The amino protons of each of the Watson−Crick base-paired cytosines were observed, with the exception of the terminal base pairs. For C^5, the 5′-neighboring base to the site of adduction, the non-hydrogen-bonded amino proton was broadened. No resonances were detected for the amino protons of C^{17}, the mismatched base opposite ${}^{R-SO}A^6$. Table S3 in the Supporting Information lists the chemical shifts of the exchangeable protons of the R(61,2)C adduct.

(b) The S(61,2)C Mismatch. The cross-peaks in the imino region of the spectrum showed connectivities between $G^2 \rightarrow G^3 \rightarrow T^{19} \rightarrow G^{18}$ and $G^8 \rightarrow T^{14} \rightarrow T^{13}$ (Figure 2). The T^{16}

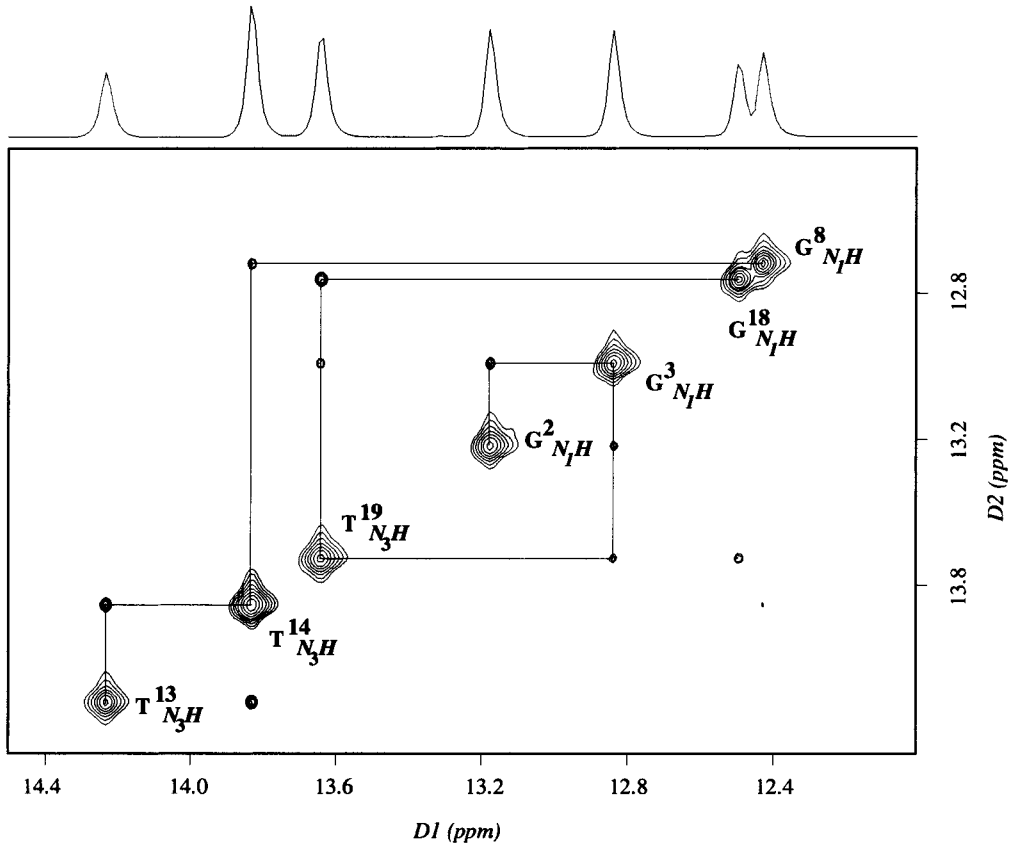

FIGURE 2: Expanded plot of a phase-sensitive NOESY spectrum for the S(61,2)C adduct (pH 7.0) at a mixing time of 350 ms showing the NOE connectivities for the imino protons of base pairs $G^{2}\cdot C^{21} \rightarrow A^{10}\cdot T^{13}$.

imino resonance, 3′ to the $^{S-SO}A^{6}\cdot C^{17}$ mismatch, was identified from its exchange with water. The T^{16} imino proton also showed a weak cross-peak to A^{7} H2. The imino protons of the terminal $C^{1}\cdot G^{22}$ and $G^{11}\cdot C^{12}$ base pairs, which exhibited rapid exchange with water, were not detected. Table S4 in the Supporting Information lists the chemical shifts of the exchangeable protons of the S(61,2)C adduct.

Styrene Protons. (a) The R(61,2)C Mismatch. The styrenyl aromatic protons were observed as two resonances at 7.21 and 7.32 ppm, which integrated in the ratio 3:2, respectively, consistent with rapid flipping of the styrenyl moiety on the NMR time scale. These two resonances showed no cross-peaks to DNA in the NOESY spectrum. The resonances of the methylene and benzylic protons were not identified.

(b) The S(61,2)C Mismatch. The styrenyl aromatic protons were observed as two resonances at 7.02 and 7.08 ppm and integrated to 2:3, respectively. The styrene aromatic protons showed cross-peaks to major groove protons in the DNA toward the 5′ direction from the lesion site. The NOE connectivities were assigned using a model based upon the observation of the 1.1 ppm ring current shielding of C^{5} H5. This suggested that C^{5} H5 was positioned above the plane of the styrene phenyl moiety. Based on the NOEs observed between the styrene aromatic protons to protons of A^{4} and C^{5} (Figure 3), it was determined that $H_{o'}$ and $H_{m'}$ should be assigned to the resonance at 7.02 ppm. Accordingly, H_{o}, H_{m}, and H_{p} were assigned to the resonance at 7.08 ppm. This led to the conclusion that flipping of the styrenyl ring in the S(61,2)C mismatch was slow on the NMR time scale. The methylene protons ($H_{\beta'}$ and $H_{\beta''}$) of the CH_2OH group resonated at 3.62 and 3.65 ppm and showed strong coupling to each other and also to both aromatic resonances of styrene. The benzylic proton of the styrene oxide moiety (H_b) was observed at 4.89 ppm that was close to the residual HDO resonance. Cross-peaks were observed between the benzylic proton and both methylene resonances. The methylene protons (3.62 and 3.65 ppm) showed strong cross-peaks to the two aromatic resonances of styrene. Strong cross-peaks were also observed between the methylene protons and T^{16} CH_3. Both methylene protons displayed weaker cross-peaks to A^{7} H1′ and C^{17} H6.

Chemical Shift Perturbations. (a) The R(61,2)C Mismatch. The primary differences between the (61,2)C mismatch and the R(61,2)C mismatch were observed at the site of the mismatch and its adjacent base pairs where the 5′ neighbor was more perturbed than the 3′ neighbor. An upfield shift of 1.69 ppm was observed for C^{5} H5 with respect to the (61,2)C mismatch. Upfield shifts of ∼0.7 ppm were also observed for C^{5} H2′ and H2″ as compared to the (61,2)C mismatch. A^{7} H1′ was shifted downfield by ∼0.2 ppm. Small upfield shifts were observed for $^{R-SO}A^{6}$ H2′ and H2″ and A^{7} H2′. In the complementary strand, C^{17} H2′ was shifted upfield by 0.3 ppm. Small downfield shifts were observed for the aromatic protons of T^{16} and C^{17} and for T^{16} CH_3.

(b) The S(61,2)C Mismatch. The primary chemical shift differences between the (61,2)C mismatch and the S(61,2)C mismatch were localized at the site of the mismatch and its 5′-neighboring base pair (Figure 4). Upfield shifts of 0.4 and 1.1 ppm were observed for C^{5} H5 and H6, respectively. An upfield shift of ∼0.35 ppm was observed for C^{5} H2′ and H2″, and a downfield shift of ∼0.3 ppm was seen for $^{S-SO}A^{6}$ H2′ and H2″ as compared to the (61,2)C mismatch. In the

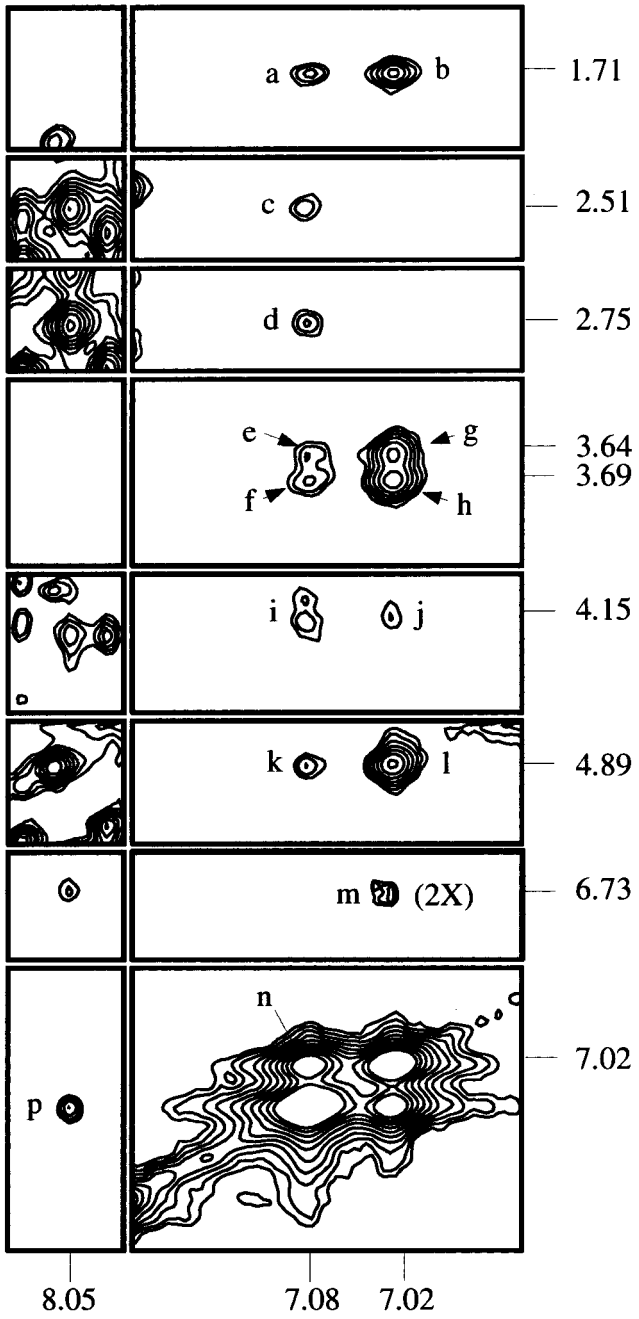

FIGURE 3: NOEs observed from the aromatic protons of styrene oxide to itself and to DNA in the S(61,2)C duplex: a, T^{16} $CH_3 \rightarrow H_m$; b, T^{16} $CH_3 \rightarrow H_{m'}$; c, A^4 H2′ $\rightarrow H_o$; d, A^4 H2″ $\rightarrow H_o$; e, $H_o \rightarrow H_{b'}$; f, $H_o \rightarrow H_{b''}$; g, $H_{o'} \rightarrow H_{b'}$; h, $H_{o'} \rightarrow H_{b''}$; i, C^5 H5 $\rightarrow H_m$; j, C^5 H5 $\rightarrow H_{o'}$; k, $H_o \rightarrow H_b$; l, $H_{o'} \rightarrow H_b$; m, C^5 H6 $\rightarrow H_{o'}$; n, $H_{m'} \rightarrow H_p$; p, A^4 H8 $\rightarrow H_m$.

complementary strand, C^{17} H1′ shifted downfield by 0.4 ppm as compared to the (61,2)C mismatch. A downfield shift was also observed for C^{12} H2′ and H2″.

Structure Refinement for the S(61,2)C Mismatch. (a) Internuclear Distances. The final experimental distance set consisted of 238 distances calculated by MARDIGRAS. Excluding the terminal base pairs, an average of 25 intranucleotide, internucleotide, and empirical distances were obtained for each base pair. The styrene−DNA cross-peaks included both first- and second-order contributions from H_o, H_m, and H_p (7.08 ppm) and $H_{o'}$ and $H_{m'}$ (7.02 ppm). A total of 264 distance restraints were used for rMD calculations. Of these, 10 were base-pairing restraints, and 16 were styrene−DNA restraints (Figure 5). Base step restraints were not used.

Table 2: Comparison of the Sixth Root Residual Indices, R_1^x, for Starting Models and Resulting rMD Structures as a Function of Mixing Time for the S(61,2)C Adduct[a,b]

	$R_1^x(\times 10^{-2})$ at			
structure	$t_m = 150$ ms[d]	$t_m = 250$ ms[d]	$t_m = 350$ ms[d]	$t_m = 350$ ms[e]
IniA[c]	22.2	21.8	20.4	16.0
IniB[c]	20.7	20.2	19.0	14.6
rMDA[c]	19.3	17.4	17.4	12.2
rMDB[c]	19.0	16.9	15.4	10.3
rMD_{final}[c]	14.1	12.2	11.2	11.6

[a] To exclude end effects, only the 9 inner base pairs were used in the calculations. [b] $R_1^x = \sum|(a_o)_i^{1/6} - (a_c)_i^{1/6}|/\sum|(a_o)_i^{1/6}|$, where (a_o) and (a_c) are the intensities of observed (nonzero) and calculated NOE cross-peaks. [c] IniA, starting energy minimized A-DNA structure; IniB, starting energy minimized B-DNA structure; rMDA, average of 5 rMD structures starting from IniA; rMDB, average of 5 rMD structures starting from IniB; rMD_{final}, average of 10 rMD structures starting from IniA and IniB. [d] Experiment performed on 500 MHz NMR. [e] Experiment performed on 750 MHz NMR.

(b) Restrained Molecular Dynamics. The rMD calculations were run without hydrogen bonding restraints imposed on the $^{S-SO}A^6 \cdot C^{17}$ mispair. Five sets of randomly seeded calculations were carried out starting from either the IniA or the IniB structures. The sets of five structures calculated from both IniA and IniB starting structures converged to a structure more similar to B-DNA, as indicated by rmsd comparison of the emergent structures to IniA and IniB. The average rmsd was 1.07 Å, with the maximum rmsd (between the two most differing structures) measured as 1.77 Å. Thus, the structural refinement procedure defined a family of closely related structures with reasonably good precision, independent of the starting coordinates. The resulting 10 rMD structures were averaged and energy minimized to obtain the final rMD structure (Figure 6).

(c) Complete Relaxation Matrix Calculations. Accuracy was evaluated by comparing the sixth root residuals between theoretical NOE intensities calculated for the emergent structures and the NMR data (Table 2). Consistent measurements of R_1^x were obtained at each of the three mixing times, with the best values being observed for the 350 ms data obtained at 750 MHz. This probably reflected the improved sensitivity of the longer mixing time data. At 350 ms, the *R*-factor for IniB was 14.6×10^{-2} as compared to a value of 16.0×10^{-2} for IniA. The *R*-factor decreased when the starting structures IniA and IniB were compared to the structures rMDA and rMDB which emerged from the calculations. The *R*-factor for the final rMD structure was 11.6×10^{-2}. The results suggested that the refined family of structures were in reasonable agreement with the NOE-based experimental restraints.

DISCUSSION

One significant finding is that protonated wobble pairing as observed in the unmodified mismatched A·C pairing interaction (*31*−*33*, *35*, *37*−*42*) does not occur in the duplex *ras61* oligodeoxynucleotide when cytosine is placed opposite either the R- or the S(61,2)-α-SO adducts. A second finding is that the structure of the mismatched A·C pairing opposite these two adducts is modulated by stereochemistry, and parallels differences observed in both the in vivo and in vitro

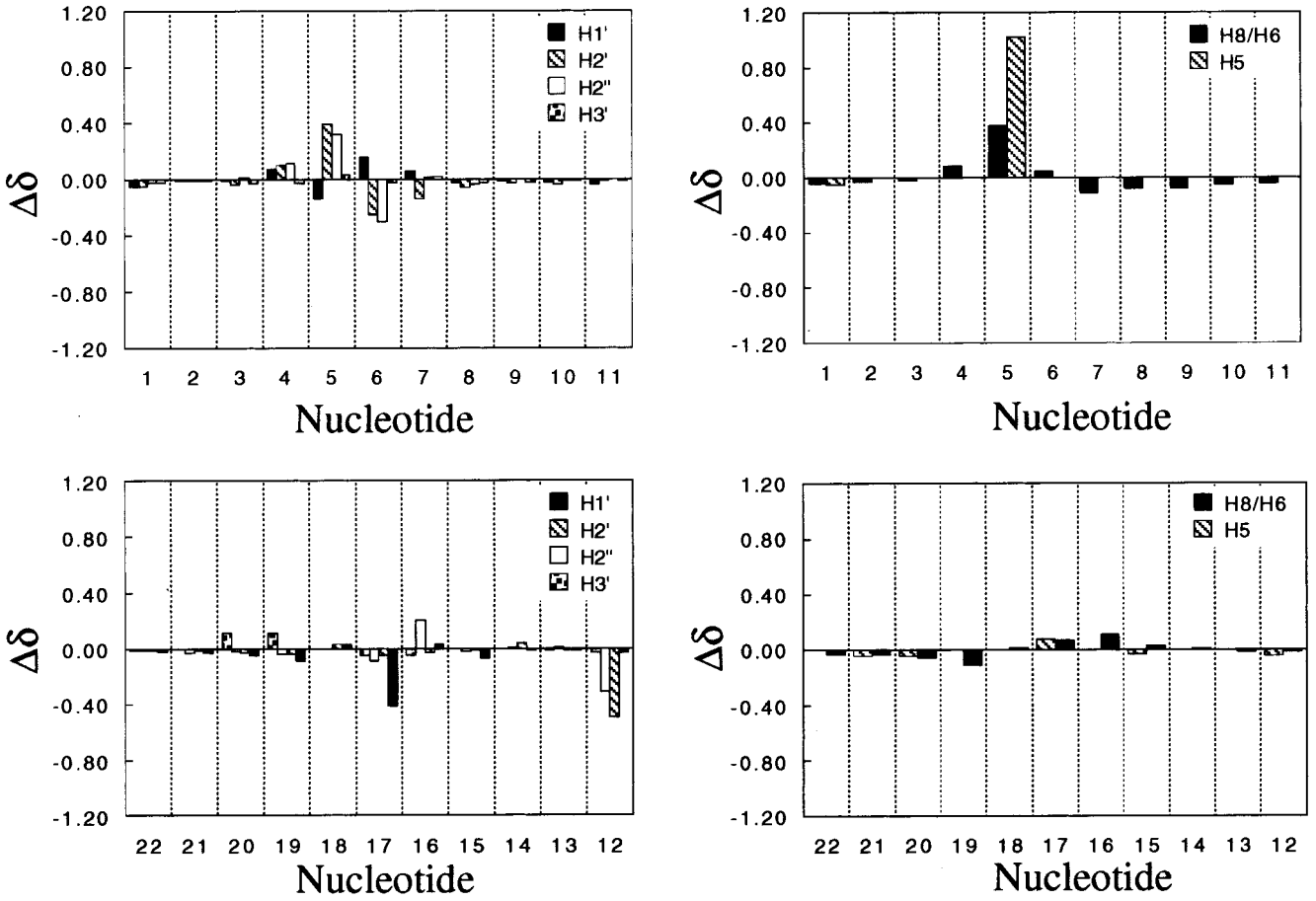

FIGURE 4: Chemical shift differences of selected protons of the S(61,2)C adduct relative to its unmodified analogue (61,2)C [$\Delta\delta = \delta_{(61,2)C} - \delta_{S(61,2)C}$].

processing of these adducts (*28*, *66*). The latter finding extends work which showed that the orientation of the α-SO adduct in the fully complementary *ras61* protooncogene sequence was dependent upon adduct stereochemistry (*44*−*46*). Thus, stereochemically dependent structural differences between these adducts both in the fully complementary duplex and when mispaired with cytosine, the putative progenitor of the A → G transition, are consistent with the differential processing of these lesions.

The R- or S(61,2)C Mismatch Pair Is Not Protonated. One striking observation was that placing $^{R-SO}A^6$ or $^{S-SO}A^6$ opposite cytosine did not result in formation of a protonated wobble A·C pairing as observed for nonadducted A·C mismatches, from crystallographic (*33*, *34*, *36*) and NMR (*31*, *32*, *35*, *37*, *39*−*42*) studies. That neither the R(61,2)C nor the S(61,2)C mismatches involved protonation of adenine was supported by the results of UV melting analyses (*38*), NMR, and the emergent rMD structures. Both the R(61,2)C and S(61,2)C mismatches exhibited decreased thermal stability at pH 5.2, which was not consistent with protonation. Examination of ^{1}H NMR spectra as a function of pH led to the same conclusion. Neither the R(61,2)C nor the S(61,2)C duplexes exhibited spectral changes upon lowering the pH to 5.2. In contrast, the unmodified (61,2)C mismatch exhibited the anticipated pH dependence of wobble pairing involving protonation of adenosine. An increase in T_m was observed at pH 5.2 as compared to pH 7.0, and the ^{1}H NMR spectrum was considerably sharper at the lower pH. The apparent pK_a was ∼7.2.

Influence of Stereochemistry. The solution structures of the mispaired R- and S(61,2)C adducts exhibited a stereochemical dependence. However, this differed from the stereochemical effect observed for the corresponding R- and S(61,2) adducts paired opposite the thymidine, the correct nucleotide. Unlike the R(61,2) adduct which exhibited a single conformation (*44*, *46*), the R(61,2)C adduct was disordered at and adjacent to the adduct site, evidenced by discontinuities in both the modified and complementary strands of the duplex in the sequential NOE connectivities expected for right-handed DNA helices, the broadening or disappearance of a number of cross-peaks from the NOE spectrum, and lower T_m as compared to the S(61,2)C adduct. The failure to observe the T^{16} N3H resonance was consistent with the conclusion that this exchangeable proton was solvent-exposed. The strong exchange peak between T^{16} N3H and water provided further evidence of solvent exposure. Thus, the 3′-neighboring base pair (A^6·C^{17}) was only weakly hydrogen bonded. The large shielding effect experienced by the 5′-neighboring cytosine, attributed to the styrenyl phenyl moiety, suggested the likelihood that the phenyl moiety remained oriented in the 5′ direction in the major groove.

Similarly, while the S(61,2) adduct exhibited multiple conformations (*45*, *46*), the S(61,2)C adduct was stabilized in a single conformation, and had a higher T_m than the R(61,2)C adduct. That both $^{S-SO}A^6$ and C^{17} were stacked was established by the ability to "walk" the NOE connectivities from C^1 to G^{11} and from C^{12} to G^{22} without interruption. T^{16} N3H was solvent-exposed, as suggested by

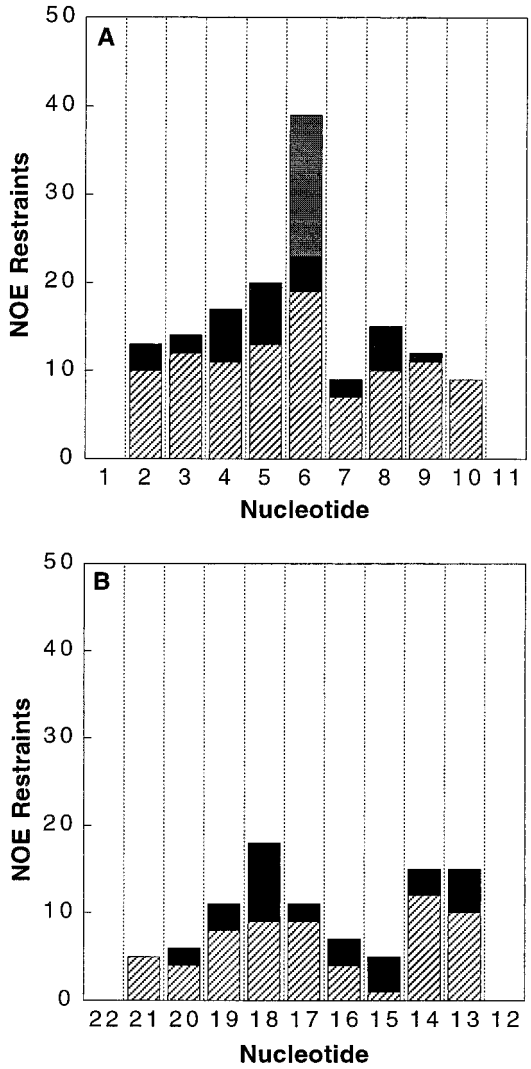

FIGURE 5: Distribution of experimental restraints between nucleotide units of the S(61,2)C adduct. The diagonally striped bars represent intranucleotide restraints while the black bars represent internucleotide and styrene−DNA restraints.

the broadening of this resonance and by the exchange peak between T^{16} N3H and water. As for the R(61,2)C adduct, the 3′-neighboring base pair was not hydrogen bonded. However, the weak cross-peak observed between T^{16} N3H and A^7 H2 suggested that the two bases were intrahelical. The 0.4 and 1.1 ppm upfield shifts observed for C^5 H5 H6 were consistent with the conclusion that these protons were proximate to the shielding cone of the styrene aromatic ring.

The observation that the S(61,2)C adduct showed NOEs to the 5′-neighbor base pair C^5·G^{18} and resulted in large upfield shifts of C^5 H5 and H6 suggested the possibility that formation of the cytosine mismatch resulted in an unexpected reorientation of the S(61,2) α-SO adduct about the adenine C6−N^6 bond or the adenine N^6−C_b bond. Such a rotation would reorient the styrene aromatic ring from the 3′-orientation to the 5′-orientation in the major groove. Inspection of the NOE data and the rMD structures for the S(61,2)C adduct revealed that this was not the case. If the styrenyl CH_2OH group were reoriented into the 3′-direction in the major groove, it might have been expected to show an NOE to T^{16} CH_3. This was not observed. Instead, T^{16} CH_3 showed NOEs to the H_m and $H_{m'}$ protons on the aromatic ring of the styrenyl moiety. The rMD structures confirmed that the CH_2-OH group remained in the 5′-direction for the S(61,2)C adduct.

The refined structure of the S(61,2)C adduct suggested the explanation for the observation of NOEs between the phenyl ring of the styrenyl moiety and the 5′-neighbor base pair C^5·G^{18}. Similar to the unadducted A·C mismatch in the (61,2)C duplex, $^{S-SO}A^6$ of the mismatch base pair in the S(61,2)C mismatch shifted toward the minor groove. This shift of the adducted adenine toward the minor groove had the effect of pulling the phenyl ring of the styrenyl moiety toward the 5′-neighbor base pair. Consequently, the C^5 H5 and H6 protons were within the shielding cone of the phenyl ring, and within NOE distance (Figure 7). This was consistent with the observation that flipping of the styrenyl ring in the S(61,2)C mismatch was slow on the NMR time scale, presumably due to the stacking interaction between the styrene ring and C^5.

Interestingly, the shift of $^{S-SO}A^6$ toward the minor groove in the S(61,2)C adduct may explain its higher T_m, as compared to the corresponding R(61,2)C adduct. Previous work suggested that for the correctly paired R(61,2) adduct, the styrenyl ring located in the major groove was proximate to the 5′-neighbor base pair (*44*, *46*). This resulted in potential steric crowding between the styrenyl ring and the 5′-neighbor base pair. Molecular modeling suggested that the cytosine mismatch-induced shift of $^{R-SO}A^6$ toward the minor groove in the R(61,2)C adduct should not be accommodated without severe distortion of the DNA duplex, consistent with the observation that the R(61,2)C adduct was disordered. It will be of interest to compare the R(61,2)C adduct with the R(*61*, *3*)C adduct, which might better be able to accommodate the altered geometry of the R(*61*, *3*)C mismatch due to the fact that the 5′-neighbor is adenine rather than cytosine. Perhaps the tendency for adenine mismatched with cytosine to shift toward the minor groove may dictate the conformation of the SO adduct in the major groove, possibly in a sequence-dependent manner.

Biological Implications. The revelation that protonated wobble A·C pairing is not observed for the R- and S(61,2)C adducts suggests that hydrogen bonding between the incoming dNTP and the DNA template may not be prerequisite to the genesis of α-SO-induced A → G mutations. This conclusion is corroborated by the observation that both the R- and S(61,2)C mismatches exhibit lower T_m values than the corresponding R- and S(61,2) adducts correctly paired with thymine, suggesting that cytosine misincorporation opposite this lesion is not favored from a thermodynamic perspective. The α-SO-induced shift of adenine toward the minor groove observed for the S(61,2)C adduct, relative to its position in an A·T Watson−Crick base pair, may play a greater role in generating these mutations. During replication, this might increase the probability of misinsertion of cytosine if the geometry of the binding pocket became more favorable for an A·C mismatch. Also, shifting adenine toward the minor groove during replication would have the effect of pulling the styrenyl moiety out of the major groove (Figure 7). It then might be less of a hindrance to subsequent extension catalyzed by the polymerase. Base-shifting has previously been proposed as a mechanism for mutagenesis induced by sterically bulky adducts (*67*−*69*). That hydrogen bonding interactions are not critical to the genesis of α-SO-

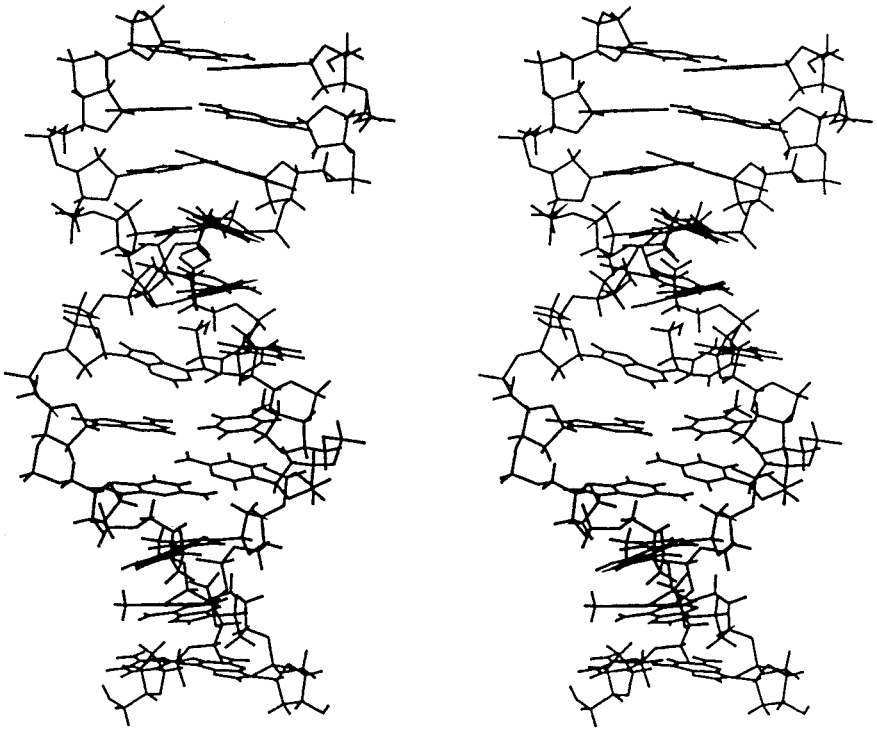

FIGURE 6: Stereoview of the refined solution structure of the S(61,2)C adduct.

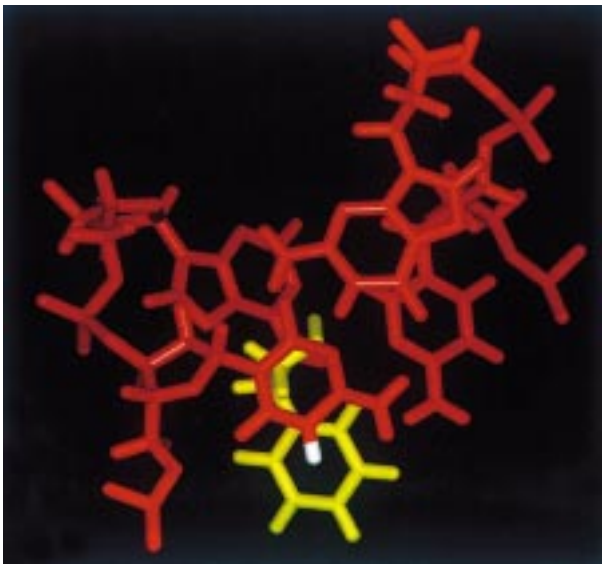

FIGURE 7: Top down view of the $C^5 \cdot G^{18}$ and $^{S-SO}A^6 \cdot C^{17}$ base pairs (yellow, styrene; white, C^5 H5).

induced A → G mutations is suggested by the observation that difluorotoluene, a geometrical analogue of thymidine lacking Watson−Crick hydrogen bonding capabilities, is easily incorporated into DNA opposite adenine. Furthermore, adenine is incorporated opposite difluorotoluene in a template strand (*70*, *71*).

The disordered structure of the R(61,2)C adduct as compared to the S(61,2)C adduct provides a potential explanation as to why the R(61,2)-α-SO adduct did not also generate low levels of A → G mutations (*28*). Due to the fact that the R(61,2)C structure is disordered, the probability of cytosine misincorporation opposite this adduct may be lower, or polymerase extension beyond the R(61,2) adduct may not be facile. Studies in vitro using HIV-1 reverse transcriptase (*72*), Klenow fragment, Sequenase 2.0, T4 polymerase holoenzyme, and human polymerases α and β revealed that replication of the R(61,2) adduct was characterized by slow kinetics of bypass synthesis (*66*). For the R(61,2) adduct, polymerization was generally terminated either opposite or one base 3′ to the adduct, although primer extension mediated by HIV-1 reverse transcriptase resulted in stop sites three bases after translesion synthesis but before reaching the end of the template (*72*). When replication was restricted to single catalytic cycles, the R(61,2) lesion presented a block to all polymerases, limiting the accumulation of fully extended primers. Bypass was facilitated in most cases when excess polymerase was used to drive the reactions (*66*).

The styrene oxide adducts provide an important model to compare and contrast with larger PAH adducts. One difference between the R- and S-α-SO adducts examined in this study and the corresponding adenyl N^6 adducts of the bulkier PAH adducts is that the α-SO adducts are located in the major groove while the PAH adducts intercalate (*73*−*79*). This may occur due to greater stacking affinity of the planar polycyclic ring in the PAH compounds. While the levels of A → G mutations induced by styrene oxide adduction within codon 61 of *N-ras* were modest, benzo[*a*]pyrene and benz-[*a*]anthracene adducts at the same positions in codon 61 caused A → G transitions at higher frequencies (*29*, *30*, *80*, *81*).

CONCLUSIONS

Placement of a cytosine mismatch opposite the R(61,2) α-SO adduct in the *ras61* oligodeoxynucleotide duplex causes a significant thermal destabilization of the R(61,2) adduct, and results in a disordered solution structure. In contrast, the corresponding cytosine mismatch opposite the S(61,2) α-SO adduct results in an ordered solution structure. Both the R- and S(61,2)C mismatches form without protonation at the mismatch site. Nevertheless, the tendency for

adenine in an A·C mismatch to shift toward the minor groove is maintained in the S(61,2)C adduct. Structural analysis of the S(61,2)C adduct provides a potential explanation as to why the S(61,2) lesion gives rise to low levels of A → G mutations while the R(61,2) lesion is nonmutagenic.

ACKNOWLEDGMENT

Dr. Hui Mao assisted with sample preparation and NMR spectroscopy. Mr. Jason P. Weisenseel assisted with structural refinement. Mr. Markus Voehler assisted with NMR spectroscopy. Dr. Mario Simeonov and Professor R. Stephen Lloyd (The University of Texas Medical Branch, Galveston) provided helpful discussions. Ms. Mary Kerske assisted with the preparation of the manuscript.

SUPPORTING INFORMATION AVAILABLE

The Supporting Information contains an accounting of the NMR data for the unmodified (61,2)C mismatch, Tables S1, the chemical shifts of the nonexchangeable protons of the R(61,2)C adduct; S2, the chemical shifts of the nonexchangeable protons of the S(61,2)C adduct; S3, the chemical shifts of the exchangeable protons of the R(61,2)C adduct; and S4, the chemical shifts of the exchangeable protons of the S(61,2)C adduct (11 pages). This material is available free of charge via the Internet at http://pubs.acs.org.

REFERENCES

1. de Meester, C., Poncelet, F., Roberfroid, M., Rondelet, J., and Mercier, M. (1977) *Mutat. Res. 56*, 147−152.
2. Wade, D. R., Airy, S. C., and Sinsheimer, J. E. (1978) *Mutat. Res. 58*, 217−223.
3. Bonatti, S., Abbondandolo, A., Corti, G., Fiorio, R., and Mazzaccaro, A. (1978) *Mutat. Res. 52*, 295−300.
4. Ott, M. G., Kolesar, R. C., Schamweber, H. C., Schneider, E. J., and Venable, J. R. (1980) *J. Occup. Med. 22*, 445−460.
5. Hodgson, J. T., and Jones, P. D. (1985) *J. Work Environ. 11*, 347−352.
6. Matanoski, G. M., and Schwarts, L. (1987) *J. Occup. Med. 29*, 675−680.
7. Wong, O. (1990) *J. Ind. Med. 47*, 753−762.
8. Harris, C., Philpot, R. M., Hernandez, O., and Bend, J. R. (1986) *J. Pharmacol. Exp. Theor. 236*, 144−149.
9. Foureman, G. L., Harris, C., Guengerich, F. P., and Bend, J. R. (1989) *J. Pharmacol. Exp. Ther. 248*, 492−497.
10. Elovaara, E., Engstrom, K., Nakajima, T., Park, S. S., Gelboin, H. V., and Vainio, H. (1991) *Xenobiotica 21*, 651−661.
11. Guengerich, F. P., Kim, D.-H., and Iwasaki, M. (1991) *Chem. Res. Toxicol. 4*, 168−179.
12. Guengerich, F. P. (1992) *FASEB J. 6*, 745−748.
13. Nelson, D. R., Kamataki, T., Waxman, D. J., Guengerich, F. P., Estabrook, R. W., Feyereisen, R., Gonzalez, F. J., Coon, M. J., Gunsalus, I. C., Goto, O., Okuda, K., and Nebert, D. W. (1993) *DNA Cell Biol. 10*, 1−51.
14. Nakajima, T., Elovaara, E., Gonzalez, F. J., Gelboin, H. V., Raunio, H., Pelkonen, O., Vainio, H., and Aoyama, T. (1994) *Chem. Res. Toxicol. 7*, 891−896.
15. Nakajima, T., Wang, R.-S., Elovaara, E., Gonzalez, F. J., Gelboin, H. V., Vainio, H., and Aoyama, T. (1994) *Biochem, Pharmacol. 48*, 637−642.
16. Savela, K., and Hemminki, K. (1986) *Arch. Toxicol. Suppl. 9*, 281−285.
17. Barlow, T., Takeshita, J., and Dipple, A. (1998) *Chem. Res. Toxicol. 11*, 838−845.
18. Qian, C., and Dipple, A. (1995) *Chem. Res. Toxicol. 8*, 389−395.
19. Latif, F., Moschel, R. C., Hemminki, K., and Dipple, A. (1988) *Chem. Res. Toxicol. 1*, 364−369.
20. Horvath, E., Prongracz, K., Rappaport, S., and Bodell, W. J. (1994) *Carcinogenesis 15*, 1309−1315.
21. Vodicka, P., Vodickova, L., and Hemminki, K. (1993) *Carcinogenesis 14*, 2059−2061.
22. Vodicka, P., Vodickova, L., Trejbalova, K., Scram, R. J., and Hemminki, K. (1994) *Carcinogenesis 15*, 1949−1953.
23. Vodicka, P., Bastlova, T., Vodickova, L., Peterkova, K., Lambert, B., and Hemminki, K. (1995) *Carcinogenesis 16*, 1473−1481.
24. Bastlova, T., Vodicka, P., Peterkova, K., Hemminki, K., and Lambert, B. (1995) *Carcinogenesis 16*, 2357−2362.
25. Bastlova, T., and Podlutsky, A. (1996) *Mutagenesis 11*, 581−591.
26. Norppa, H., Sorsa, M., Pfaffli, P., and Vainio, H. (1980) *Carcinogenesis 1*, 357−361.
27. Norppa, H., Hemminki, K., Sorsa, M., and Vainio, H. (1981) *Mutat. Res. 91*, 243−250.
28. Latham, G. J., Zhou, L., Harris, C. M., Harris, T. M., and Lloyd, R. S. (1993) *J. Biol. Chem. 268*, 23427−23434.
29. Chary, P., Latham, G. J., Robberson, D. L., Kim, S. J., Han, S., Harris, C. M., Harris, T. M., and Lloyd, R. S. (1995) *J. Biol. Chem. 270*, 4990−5000.
30. McNees, A. G., O'Donnell, M., Horton, P. H., Kim, H. Y., Kim, S. J., Harris, C. M., Harris, T. M., and Lloyd, R. S. (1997) *J. Biol. Chem. 272*, 33211−33219.
31. Patel, D. J., Kozlowski, S. A., Ikuta, S., and Itakura, K. (1984) *Biochemistry 23*, 3218−3226.
32. Patel, D. J., Kozlowski, S. A., Ikuta, S., and Itakura, K. (1984) *Fed. Proc. 43*, 2663−2677.
33. Hunter, W. N., Brown, T., Anand, N. N., and Kennard, O. (1986) *Nature 320*, 552−555.
34. Kennard, O. (1986) *Biochem. Soc. Trans. 14*, 207−210.
35. Gao, X., and Patel, D. J. (1987) *J. Biol. Chem. 262*, 16973−16984.
36. Hunter, W. N., Brown, T., and Kennard, O. (1987) *Nucleic Acids Res. 15*, 6589−6606.
37. Kalnik, M. W., Kouchakdjian, M., Li, B. F. L., Swann, P. F., and Patel, D. J. (1988) *Biochemistry 27*, 100−108.
38. Brown, T., Leonard, G. A., Booth, E. D., and Kneale, G. (1990) *J. Mol. Biol. 212*, 437−440.
39. Wang, C., Gao, H., Gaffney, B. L., and Jones, R. A. (1991) *J. Am. Chem. Soc. 113*, 5486−5488.
40. Boulard, Y., Cognet, J. A. H., Gabarro-Arpa, J., Le Bret, M., Sowers, L. C., and Fazakerley, G. V. (1992) *Nucleic Acids Res. 20*, 1933−1941.
41. Fazakerley, G. V., and Boulard, Y. (1995) *Methods Enzymol. 261*, 145−163.
42. Boulard, Y., Cognet, J. A., Gabarro-Arpa, J., Le Bret, M., Carbonnaux, C., and Fazakerley, G. V. (1995) *J. Mol. Biol. 246*, 194−208.
43. Feng, B., and Stone, M. P. (1995) *Chem. Res. Toxicol. 8*, 821−832.
44. Feng, B., Zhou, L., Passarelli, M., Harris, C. M., Harris, T. M., and Stone, M. P. (1995) *Biochemistry 34*, 14021−14036.
45. Feng, B., Voehler, M. W., Zhou, L., Passarelli, M., Harris, C. M., Harris, T. M., and Stone, M. P. (1996) *Biochemistry 35*, 7316−7329.
46. Stone, M. P., and Feng, B. (1996) *Magn. Reson. Chem. 34*, S105−S114.
47. Longnecker, D. S., and Terhune, P. G. (1998) *Pancreas 17*, 323−324.
48. Fearon, E. R., and Vogelstein, B. (1990) *Cell 61*, 759−767.
49. Loeb, L. A., and Christians, F. C. (1996) *Mutat. Res. 19*, 279−286.
50. Jen, J., Powell, S. M., Papadopoulos, N., Smith, K. J., Hamilton, S. R., Vogelstein, B., and Kinzler, K. W. (1994) *Cancer Res. 54*, 5523−5526.
51. Harris, C. M., Zhou, L., Strand, E. A., and Harris, T. M. (1991) *J. Am. Chem. Soc. 113*, 4328−4329.
52. Borer, P. N. (1975) in *Handbook of Biochemistry and Molecular Biology*, CRC Press, Cleveland.
53. Starcuk, Z., and Sklenar, V. (1985) *J. Magn. Reson. 61*, 567−570.

54. Bax, A., Sklenar, V., Clore, G. M., and Gronenborn, A. M. (1987) *J. Am. Chem. Soc. 109*, 6511−6513.
55. Sklenar, V., Brooks, B. R., Zon, G., and Bax, A. (1987) *FEBS Lett. 216*, 249−252.
56. Marion, D., Ikura, M., and Bax, A. (1989) *J. Magn. Reson. 84*, 425−430.
57. Brunger, A. T. (1992) in *X-Plor. Version 3.1. A system for X-ray Crystallography and NMR*, Yale University Press, New Haven.
58. Borgias, B. A., and James, T. L. (1990) *J. Magn. Reson. 87*, 475−487.
59. Schmitz, U., and James, T. L. (1995) *Methods Enzymol. 261*, 3−44.
60. Brooks, B. R., Bruccoleri, R. E., Olafson, B. D., States, D. J., Swaminathan, S., and Karplus, M. (1983) *J. Comput. Chem. 4*, 187−217.
61. Ryckaert, J.-P., Ciccotti, G., and Berendsen, H. J. C. (1977) *J. Comput. Phys. 23*, 327−341.
62. Keepers, J. W., and James, T. L. (1984) *J. Magn. Reson. 57*, 404−426.
63. Swaminathan, S., Ravishanker, G., Beveridge, D. L., Lavery, R., Etchebest, C., and Sklenar, H. (1990) *Proteins: Struct., Funct., Genet. 8*, 179−193.
64. Reid, B. R. (1987) *Q. Rev. Biophys. 20*, 2−28.
65. Patel, D. J., Shapiro, L., and Hare, D. (1987) *Q. Rev. Biophys. 20*, 35−112.
66. Latham, G. J., Harris, C. M., Harris, T. M., and Lloyd, R. S. (1995) *Chem. Res. Toxicol. 8*, 422−430.
67. Loechler, E. L. (1989) *Biopolymers 28*, 909−927.
68. Loechler, E. L., Benasutti, M., Basu, A. K., Green, C. L., and Essigmann, J. M. (1990) *Mutat. Environ. A*, 51−60.
69. Loechler, E. (1995) *Mol. Carcinog. 13*, 213−219.
70. Liu, D., Moran, S., and Kool, E. T. (1997) *Chem. Biol. 4*, 919−926.
71. Moran, S., Ren, R. X., and Kool, E. T. (1997) *Proc. Natl. Acad. Sci. U.S.A. 94*, 10506−10511.
72. Latham, G. J., and Lloyd, R. S. (1994) *J. Biol. Chem. 269*, 28527−28530.
73. Cosman, M., Fiala, R., Hingerty, B. E., Laryea, A., Lee, H., Harvey, R. G., Amin, S., Geacintov, N. E., Broyde, S., and Patel, D. (1993) *Biochemistry 32*, 2488−2497.
74. Cosman, M., Laryea, A., Fiala, R., Hingerty, B. E., Amin, S., Geacintov, N. E., Broyde, S., and Patel, D. J. (1995) *Biochemistry 34*, 1295−1307.
75. Schurter, E. J., Yeh, H. J. C., Sayer, J. M., Lakshman, M. K., Yagi, H., Jerina, D. M., and Gorenstein, D. G. (1995) *Biochemistry 34*, 1364−1375.
76. Schurter, E. J., Sayer, J. M., Oh-hara, T., Yeh, H. J. C., Yagi, H., Luxon, B. A., Jerina, D. M., and Gorenstein, D. G. (1995) *Biochemistry 34*, 9009−9020.
77. Yeh, H. J. C., Sayer, J. M., Liu, X., Altieri, A. S., Byrd, R. A., Lakshman, M. K., Yagi, H., Schurter, E. J., Gorenstein, D. G., and Jerina, D. M. (1995) *Biochemistry 34*, 13570−13581.
78. Zegar, I. S., Kim, S. J., Johansen, T. N., Horton, P., Harris, C. M., Harris, T. M., and Stone, M. P. (1996) *Biochemistry 35*, 6212−6224.
79. Zegar, I. S., Chary, P., Jabil, R. J., Tamura, P. J., Johansen, T. N., Lloyd, R. S., Harris, C. M., Harris, T. M., and Stone, M. P. (1998) *Biochemistry 37*, 16516−16528.
80. Chary, P., and Lloyd, R. S. (1995) *Nucleic Acids Res. 23*, 1398−1405.
81. Chary, P., Harris, C. M., Harris, T. M., and Lloyd, R. S. (1997) *J. Biol. Chem. 272*, 5805−5813.

BI9900323